Topological Materials Discovery By Large-order Symmetry Indicators

Feng Tang,[1,2] Hoi Chun Po,[3] Ashvin Vishwanath,[3] and Xiangang Wan[1,2]

[1] *National Laboratory of Solid State Microstructures and School of Physics, Nanjing University, Nanjing 210093, China*
[2] *Collaborative Innovation Center of Advanced Microstructures, Nanjing 210093, China*
[3] *Department of Physics, Harvard University, Cambridge, MA 02138, USA*

(Dated: June 12, 2018)

Crystalline symmetries play an important role in the classification of band structures, and the rich variety of spatial symmetries in solids leads to various topological crystalline phases (TCPs). However, compared with topological insulators and Dirac/Weyl semimetals, relatively few realistic materials candidates have been proposed for TCPs. Based on our recently developed method for the efficient discovery of topological materials using symmetry indicators, we explore topological materials in five space groups (i.e. $\mathcal{SG}s$**87**, **140**, **221**, **191**, **194**), which are indexed by large order strong symmetry based indicators ($\mathbb{Z}_8$ and $\mathbb{Z}_{12}$) allowing for the realization of several kinds of gapless boundary states in a single compound. We predict many TCPs, and the representative materials include: Pt_3Ge($\mathcal{SG}$**140**), graphite($\mathcal{SG}$**194**), XPt_3 ($\mathcal{SG}$**221**,X=Sn,Pb), Au_4Ti ($\mathcal{SG}$**87**) and Ti_2Sn ($\mathcal{SG}$**194**). As by-products, we also find that $AgXF_3$ ($\mathcal{SG}$**140**,X=Rb,Cs) and AgAsX ($\mathcal{SG}$**194**,X=Sr,Ba) are good Dirac semimetals with clean Fermi surface. The proposed materials provide a good platform to study the novel properties emerging from the interplay between different types of boundary states.

Since the discovery of two-dimensional (2D) and three-dimensional (3D) topological insulators (TIs), band topology in condensed-matter materials has attracted broad interest owing to their rich scientific implications and potential for technological applications [1, 2]. Described by $\mathbb{Z}_2$ topological invariant(s), time-reversal ($\mathcal{T}$) invariant TIs are characterized by an insulating gap in the bulk and $\mathcal{T}$-protected gapless modes on the boundary of the system [1, 2]. Soon after the discovery of TIs, it was realized that symmetry plays an important role in the classifications of topological phases. Based on the absence or presence of $\mathcal{T}$, particle-hole or chiral symmetry, insulators and superconductors have been classified into the so-called ten-fold periodic table [3].

In addition to the aforementioned internal symmetries, the topological classification of band structures has also been extended to include crystalline symmetries [4–6], and due to the vast array of crystal symmetries (encapsulated by the 230 crystalline space group ($\mathcal{SG}$)), massive topological crystalline phases (TCPs) have been proposed, such as: mirror Chern insulator [7], quantized electric multipole insulators [8], high order topological insulator [8–12], hourglass fermions [13], nodal-chain metals [14], unconventional quasiparticles with three-fold (or higher) band degeneracies [15] etc. Very recently, by exploiting the mismatch between the real and momentum-space descriptions of the band structure, novel forms of band topology in the 17 wallpaper groups [16], the 230 ($\mathcal{SG}s$) for nonmagnetic compounds [17, 18], and the 1651 magnetic $\mathcal{SG}s$ for magnetic materials have been proposed [19]. Currently, the standard way for finding topological materials is based on the evaluation of various topological invariants [4–7, 9, 13, 20–31]. As the calculation for topological invariants is usually a time-consuming task, the finding of any realistic topological materials is typically taken as a big success [1, 2, 6, 7, 13–15, 32–35]. The discovered topological compounds represents a very small fraction of the experimentally synthesized materials tabulated in structure databases [36]. Thus, the search for new TCPs with novel properties is of both fundamental and technological importance, and we address this issue by our recently developed method for diagnosing topological materials [37].

Our method integrates the recently established theory of symmetry indicators (SI) of band topology into first-principle band-structure calculations [16–19, 37]. As shown in Ref.[37], after standard electronic structure calculation, one needs only to calculate the representations of filled energy bands at high-symmetry points, i.e. $n^{\alpha}_{\mathbf{k}}$ which can be written as a formal vector: $\mathbf{n} = (\nu, n^1_{\mathbf{k_1}}, n^2_{\mathbf{k_1}}, \ldots)$, where ν is the total number of the filled energy bands, the subscript $\mathbf{k}_1, \mathbf{k_2}, \ldots, \mathbf{k}_N$ denotes the high symmetry point (HSP) in the BZ, the superscript $1, 2, \ldots, \alpha_i, \ldots$ refers to the irreducible representation (irrep) of little group at $\mathbf{k}_i$ point ($\mathcal{G}_{\mathbf{k}_i}$), and $n^{\alpha_i}_{\mathbf{k}_i}$ means the number of times an α_i irrep of $\mathcal{G}_{\mathbf{k}_i}$ appears among the filled bands.

It was realized that the set of vectors $\mathbf{n}$ forms an abelian group [16, 17]. Moreover, for every $\mathcal{SG}$, there exists d_{AI} atomic insulator (AI) basis vectors ($\mathbf{a}_i, i = 1, 2, \ldots, d_{\mathrm{AI}}$) containing information of the group structure for the symmetry-based indicator (SI), denoted by X_{BS} in Ref. 17, according to the possible common factor C_i for $\mathbf{a}_i$ [17]. One can always expand any vector $\mathbf{n}$ with respect to the AI basis vectors $\mathbf{a}_i$: $\mathbf{n} = \sum_{i=1}^{d_{AI}} q_i \mathbf{a}_i$. The expansion coefficients of $\mathbf{n}$ on the AI basis can be classified into three cases [37]: **Case 1**: the expansion coefficients $q_i's$ are all integers; such materials might be adiabatically connected to a trivial atomic insulator, and so we do not consider materials in this case. **Case 2**: the expansion coefficients $q_i's$ are not all integers, but all $q_iC_i's$ are integers; such materials are necessarily topological and the results of ($q_iC_i \mod C_i$), gives the nonvanishing

SI [37]. **Case 3**: the $q_i C_i's$ are not all integers; such systems are (semi-)metallic. Specifically, if $n^{\alpha}_{\mathbf{k}_i}$ is non-integer then there is band crossing happens at k_i point; on the other hand, if all the $n^{\alpha}_{\mathbf{k}}s$ are integers, then there must be band crossing in high symmetry line or plane [37].

There are various topological invariants, which correspond to different kinds of band topology. During the regular searches for topological materials, one need to decide which topological invariant to evaluate. Moreover, usually the calculations for the topological invariants are a computationally heavy task. In stark contrast to conventional target-oriented searches, our algorithm does not presuppose any specific phase of matter. Based on the expansion coefficients, which are very easy to calculate, one can quickly identify the topological (semi-)metals, topological insulators and topological crystalline insulators [37]. The high efficiency of our method has been demonstrated in Ref. 37, in which we discuss many topological materials discovered based on their nontrivial index in space groups with $\mathbb{Z}_2$ or $\mathbb{Z}_4$ strong factor in the SI group.

One of the hallmarks of topological phases is the bulk-boundary correspondence [1, 2], and different types of topological boundary states, such as Dirac surface states, hourglass surface states, and more recently hinge states, have been proposed. Thus, finding realistic materials with the coexistence of various topological boundary states is a very interesting issue. In this work we focus on $\mathcal{SG}s$ with the larger strong factor in the SI group, $X^s_{\rm BS}$, i.e., $\mathbb{Z}_8$ and $\mathbb{Z}_{12}$, where various types of band topology are expected [17, 25, 30]. These SIs are realized in $\mathcal{SG}s$ with a high-degree of coexisting symmetries, such as (roto-)inversion, mirror reflection, screw, and glide etc. There are in total 12 and 6 $\mathcal{SG}s$ with strong $\mathbb{Z}_8$ and $\mathbb{Z}_{12}$ SI factor group, respectively [17]. Focusing on five $\mathcal{SG}s$ with $\mathbb{Z}_8$ or $\mathbb{Z}_{12}$ strong SI group (i.e. $\mathcal{SG}s$ **87**, **140**, **221**, **191**, **194**), we search for interesting TCPs in a single sweep of the crystal database [36] using the method delineated in Ref. 37. We only consider spin-orbital coupled non-magnetic materials with ≤ 30 atoms in their primitive unit cell. We find a large number of TCPs with reasonably clean Fermi surfaces. In the following, we present and discuss six representative topological crystalline insulators (TCIs), and list others in Tables I and II. The 4 good Dirac semimetals are discussed in the end.

I. $\mathbb{Z}_8$ NONTRIVIAL TCI: Pt_3Ge

We first search the nonsymmorphic $\mathcal{SG}$**140** ($I4/mcm$), which has 7 AI basis vectors: $\mathbf{a}_i^{\mathcal{SG}\mathbf{140}}, i = 1, 2, \ldots, 7$. Only 2 AI basis vectors (we label them as $\mathbf{a}_6^{\mathcal{SG}\mathbf{140}}$ and $\mathbf{a}_7^{\mathcal{SG}\mathbf{140}}$) have a common factor: 2 and 8 respectively. Thus, the SI group of $\mathcal{SG}$**140** is $X_{\rm BS}^{\mathcal{SG}\mathbf{140}} = \mathbb{Z}_2 \times \mathbb{Z}_8$. There are 158 materials with small unit cell and without magnetic atoms. The calculations based on our method [37] identified 77 topological nontrivial compounds, with 27 belonging to case 2 while 50 being topological (semi-)metals indicated by case 3. Further filtering by Fermi level criteria which requires that the energy bands around the Fermi level are clean as far as possible, we list the relatively good materials in Table I. In the following, we take Pt_3Ge [38] as the example to analyze the detailed topological properties.

$\mathcal{SG}$	$X_{\rm BS}$	material(SI)
87	$\mathbb{Z}_2 \times \mathbb{Z}_8$	Au_4Ti
140	$\mathbb{Z}_2 \times \mathbb{Z}_8$	Pt_3Ge(04),$SiTa_2$(11)
221	$\mathbb{Z}_4 \times \mathbb{Z}_8$	AlX(X=Sc,Y)(03) XB_6(X=Ca,Sr,Ba)(03) BeTi(03), CaPd(20),$CsPbBr_3$(23) $CsGeBr_3$(23),$CsSnI_3$(23) Ca_3PbO(22),XPt_3(X=Pb,Sn)(34)

TABLE I. The topological crystalline (TC) insulating materials for $\mathcal{SG}s$**87**, **140** and **221**. These $\mathcal{SG}s$ all own the same strong SI factor group: $\mathbb{Z}_8$ but with different other weak SI factor groups. The red color denotes the materials carefully discussed in this work.

$\mathcal{SG}$	$X_{\rm BS}$	material(SI)
191	$\mathbb{Z}_6 \times \mathbb{Z}_{12}$	XB_2(X=Mg,Ca)(52),SrB_2(15),Ti(33)
194	$\mathbb{Z}_{12}$	AlLi(4),AlC_2Ta_3(1),Ca_2NI(3) graphite(4),Na_2CdSn(4) MgPo(1),$SiSr_2$(1) Ti_2Sn(6)

TABLE II. The TC insulating materials for $\mathcal{SG}s$**191** and **194**. These $\mathcal{SG}s$ all own the same strong SI factor group: $\mathbb{Z}_{12}$ but with different other weak SI factor groups. The red color denotes the materials carefully discussed in this work.

Pt$_3$Ge crystallize in the body-centered tetragonal structure [38], where Ge occupies the 4b Wyckoff position, and Pt's occupying two sets of inequivalent sites in the 4a and 8h Wyckoff positions. There are in total 68 valence electrons in the primitive unit cell. Based on *ab initio* calculation, we calculate the irrep multiplicities $n^{\alpha}_{\mathbf{k}}s$ for all the high symmetry points and all the corresponding irreps α for the 68 valence bands. We then expand this calculated vector $\mathbf{n}$ on the 7 AI basis vectors:

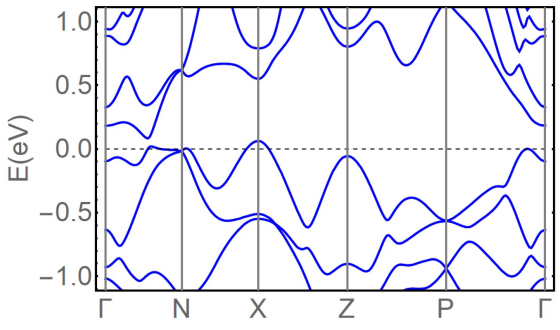

FIG. 1. The electronic band plot of TCI Pt_3Ge within $\mathcal{SG}$**140**.

$\mathbf{n} = \sum_{i=1}^{7} q_i \mathbf{a}_i^{\mathcal{SG}\mathbf{140}}$, and obtain $q = (8, 0, 0, 1, 2, 1, -\frac{1}{2})$. Thus this material belongs to case 2, and is a TCI with SI being (0,4). As seen from the electronic band plot in Fig. 1, this material has large direct gaps through the k path.

While from SI alone we can ascertain that Pt_3Ge is a TCI, to resolve the concrete form of band topology it displays we have to evaluate additional topological indices. First, we note that from the SI we can infer all the Fu-Kane parity criterion [21] is silenced, i.e., the material cannot be a strong nor weak TI. The enriched inversion invariant δ_i [25, 30] ($\delta_i \equiv (\kappa_1 \mod 4)/2$) is also vanishing. Thus this material has boundary states protected by symmetry operation containing $n-$fold axis ($n > 1$) [25, 30]. Due to the rich point symmetry operations in $\mathcal{SG}\mathbf{140}$ (whose point group is D_{4h}), several topological phases may occur [25, 30]. We thus evaluate the mirror Chern numbers for the (001) (Miller indices with respect to the conventional lattice basis vectors) and (110)-mirror planes by first principles calculations. Our numerical results show that they are also all vanishing. The glide, screw and S_4 invariant is thus nonvanishing [25, 30]. Thus it would have glide protected hourglass surface states in (100) glide symmetric planes as the corresponding invariant is 1. The (001) screw invariant is 1 thus it would protect gapless hinge states along the $\mathbf{c}$ direction.

II. $\mathbb{Z}_{12}$ NONTRIVIAL TCI: GRAPHITE

We also searched the 492 materials with $\mathcal{SG}\mathbf{194}(P6_3/mmc$, whose point group is $D_{6h})$ in the database[36]. There are 52 and 254 materials belonging to cases 2 and 3 respectively. It is worth emphasizing that our results indicate that graphite [39] is potentially a nontrivial insulator.

It is well-known that graphene (i.e. monolayer of graphite) exhibits 2D massless Dirac excitation near K/K' points [40]. The spin-orbit (SO) coupling (although small), opens a topological gap ($\sim$0.0008 meV [41]), making it, in principle, a 2D topological insulator [42]. The direct stacking of graphene will then lead to a weak topological insulator. The discovery of crystalline-symmetry-protected band topology in graphite, the ABABABAB... Bernal stacking of graphene, demonstrates the possibilities of discovering topological materials even among the simplest elemental materials. We thus present a detailed discussion in the following.

The $\mathcal{SG}\mathbf{194}$ owns 13 AI basis vectors $\mathbf{a}_i^{\mathcal{SG}\mathbf{194}}, i = 1, 2, \ldots, 13$, where only the last one has a common factor, which is 12. Thus $X_{\rm BS}^{\mathcal{SG}\mathbf{194}} = \mathbb{Z}_{12}$. The 16 valence bands in graphite are found to have the expansion coefficients $q = (2, 0, -1, -1, -1, -1, 1, 3, \frac{1}{3})$ on the AI basis. Thus the SI for graphite is $4 \in \mathbb{Z}_{12}$. The band structure is shown in Fig. 2, where SO coupling opens a small gap (around 0.025 meV) at the K point. The inversion invariant δ_i and three Fu-Kane weak topological invariants [21] are found to be all vanishing. We then calculate the (001)-mirror Chern number and find that it is -2. Thus there would be gapless Dirac surface states in the (001) mirror symmetric planes. In order to ascertain graphite's nontrivial topology, we then calculate the $(\bar{1}20)$ plane's mirror Chern, and find that it is vanishing. Then it would has 6-fold screw protected hinge states [25, 30]. It may also have glide and rotation protected surface states as dictated by the nonvanishing $\{c_2^{1\bar{1}0}|000\}$ (in Seitz notation where the superscript of the point operation part denotes that rotation axis and the subscript denotes the rotation angle) rotation invariant and (010) glide invariant [25, 30]. While graphite is generally associated with small Fermi pockets, Ref. [43] proposed, based on the observation of a semiconducting gap in small samples of Bernal graphite, that these may arise from extrinsic effects. Thus , further experimental work would be of great interest.

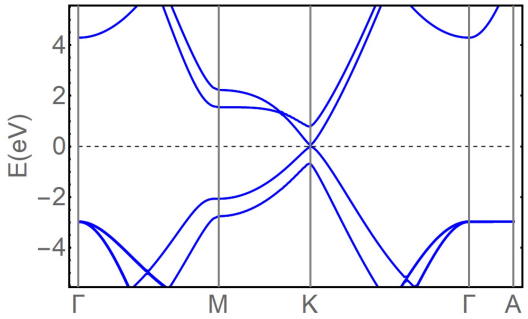

FIG. 2. The electronic band plot of TCI graphite within $\mathcal{SG}\mathbf{194}$.

III. THE OTHER DISCOVERED TCIS

A. Weak TI coexisting with TCI in $PbPt_3$($\mathcal{SG}$221) and Au_4Ti($\mathcal{SG}$87)

The above two TC materials both have vanishing inversion and weak topological invariants. We also discover two materials, i.e. $PbPt_3$ in $\mathcal{SG}\mathbf{221}$ and Au_4Ti in $\mathcal{SG}\mathbf{87}$ which have three weak topological indices [21] $\nu_i = 1$ for $i = 1, 2, 3$: they have inversion topological invariant δ_i [25, 30] equal to 0 and 1, respectively.

$PbPt_3$ crystallizes in the cubic structure with a primitive Bravais lattice. The electronic band structure is shown in Fig. 3. The material has 34 valence electrons in the unit cell. The calculated $n_{\mathbf{k}}^{\alpha}$'s for these 34 bands can be expanded on the 14 AI basis vectors of $\mathcal{SG}\mathbf{221}$, and the expansion coefficients are $q = (0, 0, 0, 0, 0, -1, 1, 1, 0, 1, -1, -1, -\frac{1}{4}, -\frac{1}{2})$. The last two AI basis vectors own a common factor 4 and 8, respectively. Thus the SI is $(3, 4) \in \mathbb{Z}_4 \times \mathbb{Z}_8$. The parity calculations show that it is a weak topological insulator [21]. We also calculate the two mirror Chern numbers for (001)

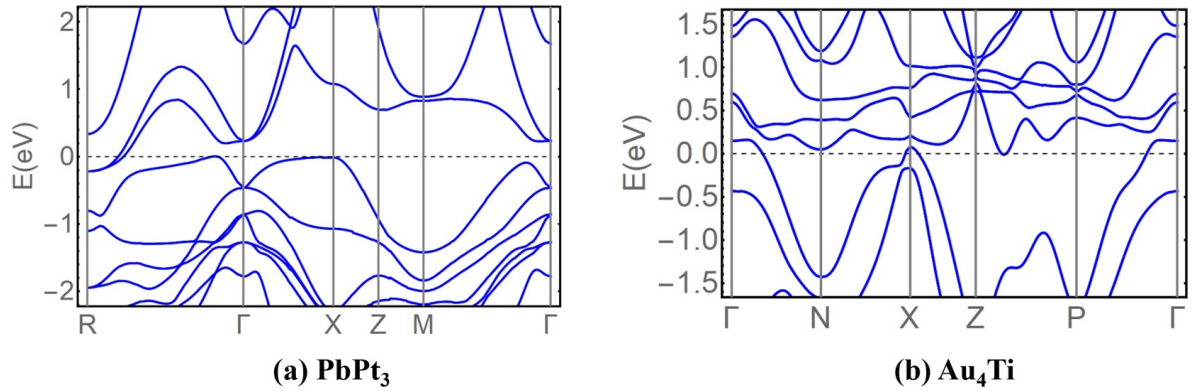

FIG. 3. The electronic band plots of TCIs $PbPt_3$ within $\mathcal{SG}$**221** and Au_4Ti within $\mathcal{SG}$**87** .

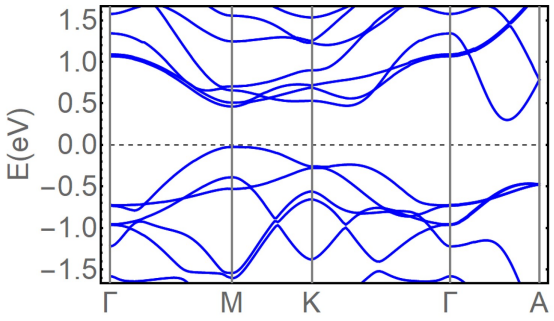

FIG. 4. The electronic band plot of TCI Ti_2Sn within $\mathcal{SG}$**194**.

mirror plane ($k_z = 0$ or π), and find that they are both equal to -1. At the same time, the screw invariant of $\{c_2^{011}|0\frac{1}{2}\frac{1}{2}\}$ is 1. Thus this material can host protected hinge and surface states at the same time.

Au_4Ti [44] crystallizes in $\mathcal{SG}$**87** ($I4/m$), where Au and Ti occupy $8h$ and $2a$ Wyckoff positions respectively. This material is found to belong to case 2. We calculate the parities and find that its strong topological invariant [21] and inversion invariant [25, 30] are both vanishing i.e., $\nu_0 = \delta_i = 0$ while $\nu_1 = \nu_2 = \nu_3 = 1$, so it is a weak TI. Besides, the newly introduced invariant Δ [25] is found to be 4 (mod 8). Our first principles calculations also show that the mirror Chern number for the (001)-plane is vanishing. Thus it would allow glide protected hourglass surface states in glide $\{m_{001}|\frac{1}{2}\frac{1}{2}0\}$ symmetric plane. It can also host hinge states along (001) direction which are protected by screw $\{c_2^{001}|00\frac{1}{2}\}$ or $\{c_4^{001}|00\frac{1}{2}\}$.

B. TCI Ti_2Sn in $\mathcal{SG}$194

Ti_2Sn [45] within $\mathcal{SG}$**194** is found to be a TCI. It has large direct gaps everywhere except in a small area where there are little electron and hole pockets. Our calculation show that the SI is (6). Parity calculations show that the inversion invariant δ_i [25, 30] is 1 while the strong and weak topological invariants [21] $\nu_{0,1,2,3}$ are all vanishing. From first principles calculation, we find the mirror Chern number for the $(\bar{1}20)$ plane is -4. This high mirror Chern number indicates that there should be multiple Dirac cones in the $(\bar{1}20)$ mirror symmetric plane. In order to identify the band topology, we also calculate the mirror Chern number of the (001) mirror plane, which is found to be vanishing. Thus it can accommodate hourglass surface states in $\{m_{010}|00\frac{1}{2}\}$ or $\{m_{010}|\frac{1}{2}0\frac{1}{2}\}$ glide symmetric planes. c_2 around (010) can also protect surface Dirac cones. Besides, inversion and screw $\{c_6^{001}|00\frac{1}{2}\}$ can protect hinge states in corresponding hinges satisfying the corresponding symmetries.

IV. TOPOLOGICAL SEMIMETALS

Other than the TCIs, our method can also filter out topological (semi-)metals when the expansion coefficients belong to case 3. By further requiring relatively clean Fermi surfaces, we identify $AgXF_3$[46](X=Rb,Cs,$\mathcal{SG}$**140**) as good Dirac semimetals with Dirac points pinned down to two high symmetry points (P and N), and AgAsX[47, 48](X=Sr,Ba,$\mathcal{SG}$**194**) as Dirac semimetals with symmetry-protected band crossing at high symmetry line, as shown in Fig. 5. These two materials families realize the two sub-cases within case 3 that we discussed. For the $AgXF_3$ family, the high symmetry points P and N both have only one 4-dimensional irrep while the filling cannot be divided by 4. The filling-enforced Dirac points at P or N are subjected to more symmetry restrictions than those for the Dirac points in high symmetry line, and consequently the Dirac dispersion is more isotropic. For the AgAsX family, in the high symmetry line Γ-A, the Δ_7 and Δ_9 band crossing each other, resulting a Dirac point protected by C_{6v}. The Fermi level exactly threads the Dirac point.

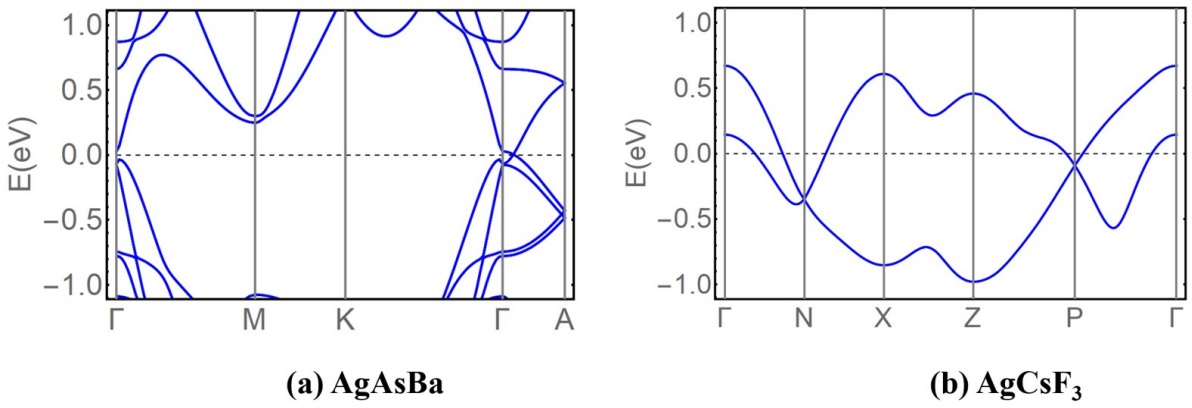

FIG. 5. The electronic band plots of Dirac semimetals AgAsBa within $\mathcal{SG}$**194** and $AgCsF_3$ within $\mathcal{SG}$**140** .

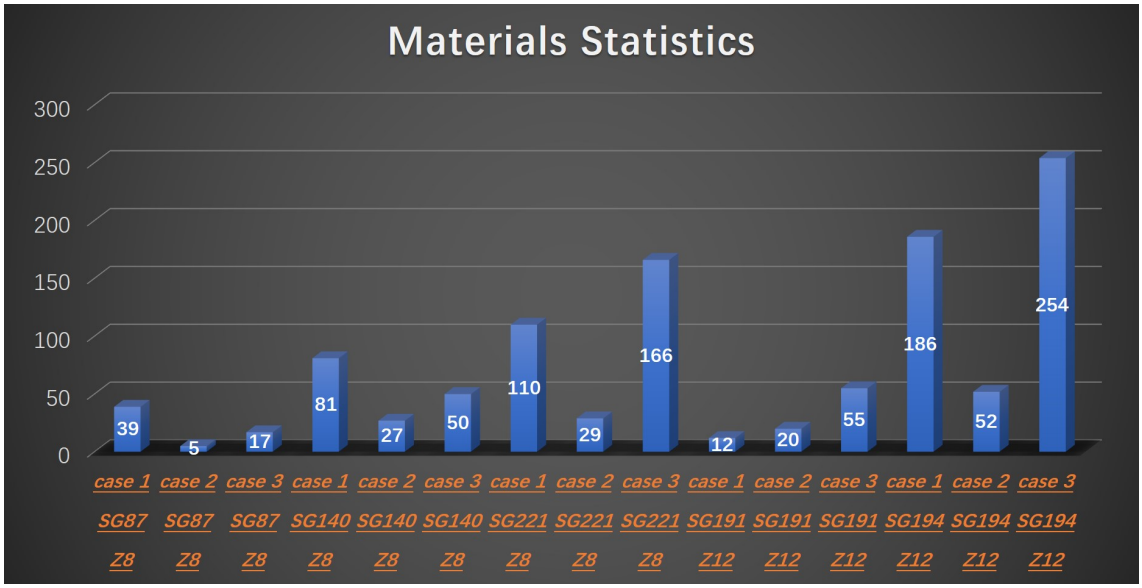

FIG. 6. The statistics of topological materials search using the SI method. The number in each bar indicates the number of materials for each case. Case 1 corresponds to the trivial situation, while case 2 and 3 correspond to topological band structures and semimetals respectively. Requiring a minimal Fermi surface further reduces the number of viable candidates.

V. CONCLUSIONS AND PERSPECTIVES

In this work, based on our newly developed algorithm [37], we search for topological materials indicated by $\mathbb{Z}_8$ and $\mathbb{Z}_{12}$ strong factors in the SI groups. Focusing on $\mathcal{SG}s$**87**, **140**, **221**, **191**, **194**, we predict many materials, which exhibit coexistence of various gapless boundary states due to the rich combination of various symmetry operators in these highly symmetric $\mathcal{SG}s$. Breaking the symmetry operation directly affects (move or even gap) the gapless topological boundary state, thus one may easily tune the novel properties of these predicted topological materials through strain or boundary decoration.

It is worth mentioning that the electronic topological phenomenon is widespread in real materials and as shown in the Fig. 6, majority of the materials in the five $\mathcal{SG}s$ we scanned belong to topological phases indicated by cases 2 and 3. In this manuscript, we only discuss the materials with clean Fermi surfaces, since in these materials we expect the transport properties to be dominated by the topologically non-trivial states. Our scheme also finds some good metal with big Fermi surfaces possessing nonzero SI. One good example is MgB_2. It is interesting to contemplate on the possible interplay between its superconductivity [49] and band topology.

We hope that our proposed materials will enrich the set of realistic topological crystalline materials and stimulate related experiments. With the demonstrated efficiency,

our method [37] can be employed for a large-scale systematic search of the entire materials database, which could lead to the discovery for many more new topological materials.

ACKNOWLEDGMENTS

FT and XGW were supported by National Key R&D Program of China (No. 2017YFA0303203 and 2018YFA0305700), the NSFC (No. 11525417, 51721001 and 11790311). FT was also supported by the program B for Outstanding PhD candidate of Nanjing University. XGW was partially supported by a QuantEmX award funded by the Gordon and Betty Moore Foundation's EPIQS Initiative through ICAM-I2CAM, Grant GBMF5305 and by the Institute of Complex Adaptive Matter (ICAM). AV is supported by NSF DMR-1411343, a Simons Investigator Grant, and by the ARO MURI on topological insulators, grant W911NF- 12-1-0961.

[1] M. Z. Hasan and C. L. Kane, Rev. Mod. Phys. **82**, 3045 (2010).
[2] X. L. Qi, and S. C. Zhang, Rev. Mod. Phys. **83**, 1057 (2011).
[3] C.-K. Chiu, J. C. Y. Teo, A. P. Schnyder and S. Ryu, Rev. Mod. Phys. **88**,035005 (2016).
[4] L. Fu, Phys. Rev. Lett. **106**, 106802 (2011).
[5] R.-J. Slager, A. Mesaros, V. Juričić and J. Zaanen, Nature Phys. **9**, 98 (2013).
[6] Y. Ando and L. Fu, Annu. Rev. Condens. Matter Phys. **6**, 361 (2015).
[7] T. H. Hsieh, H. Lin, J. Liu, W. Duan, A. Bansil and L. Fu, Nat. Commun. **3**, 982 (2012).
[8] W. A. Benalcazar, B. A. Bernevig, T. L. Hughes, Science **357**, 61 (2017).
[9] F. Schindler, A. M. Cook, M. G. Vergniory, Z. Wang, S. S. P. Parkin, B. A. Bernevig and T. Neupert, Science Adv. **4**, eaat0346 (2018).
[10] W. A. Benalcazar, B. A. Bernevig, and T. L. Hughes, Phys. Rev. B. **96**, 245115 (2017).
[11] Z. Song, Z. Fang, and C. Fang, Phys. Rev. Lett. **119**, 246402 (2017).
[12] J. Langbehn, Y. Peng, L. Trifunovic, F. von Oppen, and P. W. Brouwer, Phys. Rev. Lett. **119**, 246401 (2017).
[13] Z. Wang, A. Alexandradinata R. J. Cava and B. A. Bernevig, Nature **532**, 189 (2016).
[14] T. Bzdušek, Q. Wu, A. Rüegg, M. Sigrist and A. A. Soluyanov, Nature **538**, 75 (2016).
[15] B. Bradlyn, J. Cano, Z. Wang, M. G. Vergniory, C. Felser, R. J. Cava, B. A. Bernevig, Sciences **353**, aaf5037 (2016).
[16] J. Kruthoff, J. de Boer, J. van Wezel, C. L Kane and R. J. Slager, Phys. Rev. X **7**, 041069 (2017).
[17] H. C. Po, A. Vishwanath, H. Watanabe, Nat. Commun. **8**, 50 (2017).
[18] B. Bradlyn, L. Elcoro, J. Cano, M. G. Vergniory, Z. Wang, C. Felser, M. I. Aroyo and B. Andrei Bernevig, Nature **547**, 298 (2017).
[19] H. Watanabe, H. C. Po, and A. Vishwanath, arXiv:1707.01903 (2017).
[20] B. J. Wieder, B. Bradlyn, Z. Wang, J. Cano, Y. Kim, H.-S. D. Kim, A. M. Rappe, C. L. Kane and B. A. Bernevigm, arXiv:1705.01617 (2017).
[21] L. Fu and C. L. Kane, Phys. Rev. B **76**, 045302 (2007).
[22] C. Fang and L. Fu, arXiv:1709.01929 (2017)
[23] J. Langbehn, Y. Peng, L. Trifunovic, F. von Oppen, and P. W. Brouwer, Phys. Rev. Lett. **119**, 246401 (2017).
[24] W. A. Benalcazar, B. A. Bernevig, and T. L. Hughes, Phys. Rev. B **96**, 245115 (2017).
[25] E. Khalaf, H. C. Po, A. Vishwanath, and H. Watanabe, arXiv:1711.11589 (2017).
[26] E. Khalaf, arXiv:1801.10050 (2018).
[27] Max Geier, Luka Trifunovic, Max Hoskam and Piet W. Brouwer, arXiv: 1801.10053 (2018).
[28] C. Fang, M. J. Gilbert and B. A. Bernevig, Phys. Rev. B **86**, 115112 (2012).
[29] C. Fang and L. Fu, Phys. Rev. B **91**, 161105 (2015).
[30] Z. Song, T. Zhang, Z. Fang and C. Fang, arXiv: 1711.11049 (2017).
[31] C. Fang, Z. Song and T. Zhang, arXiv:1711.11050 (2017).
[32] X. Wan, A. M. Turner, A. Vishwanath, and S. Y. Savrasov, Phys. Rev. B **83**, 205101 (2011).
[33] H. Weng, C. Fang, Z. Fang, B. A. Bernevig, and X. Dai, Phys. Rev. X **5**, 011029 (2015).
[34] S.-M. Huang, S.-Y. Xu, I. Belopolski, C.-C. Lee, G. Chang, B. Wang, N. Alidoust, G. Bian, M. Neupane, C. Zhang, S. Jia, A. Bansil, H. Lin, and M. Z. Hasan, Nat. Commun. **6**, 7373 (2015).
[35] X. Zhou, C.-H Hsu, T.-R. Chang, H.-J. Tien, Q. Ma, P. Jarillo-Herrero, N. Gedik, A. Bansil, V. M. Pereira, S.-Y. Xu, H. Lin, and L. Fu, arXiv:1805.05215 (2018).
[36] M. Hellenbrandt, Crystallography Reviews **10**, 17 (2004).
[37] F. Tang, H. C. Po, A. Vishwanath, and X. Wan, arXiv:1805.07314 (2018).
[38] M. Ellner and B. Predel, Zeitschrift fuer Metallkunde **51**, 327 (1960).
[39] B. Vadlamani, K. An, M. Jagannathan and K. S. R. Chandran, J. Electrochemical Society **161**, A1731 (2014).
[40] A. H. Castro Neto, F. Guinea, N. M. R. Peres, K. S. Novoselov, and A. K. Geim, Rev. Mod. Phys. **81**, 109 (2009).
[41] Y. Yao, F. Ye, X.-L. Qi, S.-C. Zhang, and Z. Fang, Phys. Rev. B 75, 041401 (2007).
[42] C. L. Kane and E. J. Mele, Phys. Rev. Lett. **95**, 226801 (2005).
[43] N Garca, P Esquinazi, J Barzola-Quiquia and S Dusari, New J. Phys. 14 053015 (2012).

[44] P. Pietrokowsky, Journal of the Institute of Metals **90**, 434 (1962).
[45] C. Colinet, J. C. Tedenac and S. G. Fries, Comouter coupling of phase diagrams and thermochemistry **33**, 250 (2009).
[46] R. H. Odenthal and R. Hoppe, Monatshefte fuer Chemie **102**, 1340 (1971).
[47] A. Mewis, Zeitschrift fuer Naturforschung, Teil B. Anorganische Chemie, Organische Chemie **33**, 983 (1978).
[48] A. Mewis, Zeitschrift fuer Naturforschung, Teil B. Anorganische Chemie, Organische Chemie **34**, 1373 (1979).
[49] J. Nagamatsu, N. Nakagawa, T. Muranaka, Y. Zenitani, and J. Akimitsu, Nature **410**, 63 (2001).